Mineralogical Magazine, December 2018, Vol. 82(6), pp. 1261–1275

Redcanyonite, $(NH_4)_2Mn[(UO_2)_4O_4(SO_4)_2](H_2O)_4$, a new zippeite-group mineral from the Blue Lizard mine, San Juan County, Utah, USA

Travis A. Olds[1,*], Jakub Plášil[2], Anthony R. Kampf[3], Peter C. Burns[1,4], Barbara P. Nash[5], Joe Marty[6], Timothy P. Rose[7] and Shawn M. Carlson[8]

[1] Department of Civil and Environmental Engineering and Earth Sciences, University of Notre Dame, Notre Dame, IN 46556, USA
[2] Institute of Physics ASCR, v.v.i., Na Slovance 1999/2, 18221 Prague 8, Czech Republic
[3] Mineral Sciences Department, Natural History Museum of Los Angeles County, 900 Exposition Boulevard, Los Angeles, CA 90007, USA
[4] Department of Chemistry and Biochemistry, University of Notre Dame, Notre Dame, IN 46556, USA
[5] Department of Geology & Geophysics, University of Utah, Salt Lake City, UT 84108, USA
[6] 5199 East Silver Oak Road, Salt Lake City, UT 84108, USA
[7] Nuclear and Chemical Sciences Division, Lawrence Livermore National Laboratory, Livermore, CA 94550, USA
[8] 245 Jule Lake Road, Crystal Falls, MI 49920, USA

[*Received 23 July 2017; Accepted 15 November 2017; Associate Editor: Giancarlo Della Ventura*]

ABSTRACT

Redcanyonite (IMA2016-082), $(NH_4)_2Mn[(UO_2)_4O_4(SO_4)_2](H_2O)_4$, occurs underground in the Blue Lizard mine, Red Canyon, White Canyon district, San Juan County, Utah, USA. It occurs with natrozippeite, brochantite, devilline, posnjakite, johannite, gypsum, bobcookite, pickeringite, pentahydrite and the NH_4-analogue of zippeite: ammoniozippeite. Redcanyonite occurs as radial aggregates of red–orange needles and blades individually reaching up to 0.2 mm long, with aggregates measuring up to 1 mm in diameter. Crystals are flattened on {010} and elongated along [100], exhibit perfect cleavage on {010}, and exhibit the forms {010}, {001}, {101} and {10$\bar{1}$}. Twinning is ubiquitous, by 180° rotation on [100]. Redcanyonite is translucent with a pale orange streak, is non-fluorescent, has a Mohs hardness of 2, and has brittle tenacity with uneven fracture. Optically, redcanyonite is biaxial (+), $\alpha = 1.725(3)$, $\beta = 1.755(3)$, $\gamma = 1.850(5)$ (white light); 2V (meas.) = 60(2)°, 2V (calc.) = 61.3°; and dispersion is $r < v$, very strong. Pleochroism is: X = orange, Y = yellow and Z = orange; $Y << X < Z$. The optical orientation is $X = b$, $Y \approx c^*$, $Z \approx a$. The empirical formula is $(NH_4)_{2.02}(Mn_{0.49}Cu_{0.09}Zn_{0.06})_{\Sigma 0.64}H^+_{0.72}[(UO_2)_4O_4(S_{0.99}P_{0.01}O_4)_2](H_2O)_4$, based on 4 U and 24 O apfu. Redcanyonite is monoclinic, $C2/m$, $a = 8.6572(17)$, $b = 14.155(3)$, $c = 8.8430(19)$ Å, $\beta = 104.117(18)°$, $V = 1050.9(4)$ Å^3 and $Z = 2$. The structure was refined to $R_1 = 0.0382$ for 1079 reflections with $I_{obs} > 3\sigma I$. Uranyl oxo-sulfate sheets in redcanyonite adopt the well-known zippeite topology, which consists of zigzag chains of uranyl pentagonal bipyramids linked by sulfate tetrahedra to form sheets. The sheets are linked to each other through bonds to interlayer NH^+_4 groups and octahedrally coordinated Mn^{2+}, and by hydrogen bonds from H_2O groups. Redcanyonite is named for Red Canyon in southeast Utah, USA.

Keywords: redcanyonite, new mineral, uranium, zippeite group, uranyl sulfate, crystal structure, Blue Lizard mine.

*E-mail: toldxls@gmail.com
https://doi.org/10.1180/minmag.2017.081.094

Introduction

Uranium is commonly deposited in geochemical environments where a solution containing U^{6+} is met by reducing conditions created by organic matter, ferrous-iron minerals or sulfides, leading to precipitation of uraninite (Langmuir, 1978). Oxidizing groundwater can re-solubilize uranium and alter sulfides, leading to the formation of sulfate (Garrels and Christ, 1959; Finch and Murakami, 1999; Plášil, 2014). Subsequent evaporation in the presence of cations (e.g. Na^+, K^+ or Mg^{2+}) can lead to crystallization of uranyl sulfate minerals, most commonly those of the zippeite group (Brugger *et al.*, 2003). The majority of natural and synthetic analogues of zippeite-group minerals have refined structures and crystal-chemical variations observed in the group are well-established (Burns *et al*., 2003; Brugger *et al.*, 2006; Peeters *et al*., 2008; Plášil *et al.*, 2011*a*,*b*, 2013, 2014; Plášil, 2015; Plášil and Škoda, 2015; Plášil *et al.,* 2017, 2018). The interlayer composition and configuration of group members is diverse, due to the ability of the zippeite sheet to shift its charge and accommodate variable amounts of monovalent, divalent, and even trivalent cations. Redcanyonite is a new NH_4 and Mn-bearing member of the zippeite group, which now includes 12 unique minerals.

Redcanyonite is named after Red Canyon in southeast Utah, and alludes to the red and orange hues of iron-stained sandstones within the canyon, which are also adopted in the striking colour of the new mineral. Red Canyon is the type locality for 22 recently-described uranium minerals, with several more currently under study that we are aware of. The region has produced a remarkable number of unique uranyl minerals that are only found there; in particular, several uranyl sulfates. Extensive oxidation of ore minerals (uraninite and sulfides) coupled with inflow of dry desert air has favoured crystallization of uranyl minerals. Episodic dissolution and re-precipitation occurring between wet and dry periods augments the complexity and diversity of uranyl sulfates found there.

The mineral and its name were approved by the Commission on New Minerals, Nomenclature and Classification of the International Mineralogical Association (IMA2016-082). Six co-type specimens are deposited in the collections of the Natural History Museum of Los Angeles County, 900 Exposition Boulevard, Los Angeles, CA 90007, USA, under the catalogue numbers 66293, 66294, 66295, 66296, 66297 and 66298.

Occurrence

Redcanyonite occurs underground in the Blue Lizard mine, Red Canyon, White Canyon mining district, San Juan County, Utah (37°33'26"N, 110° 17'44"W). Red Canyon is located in west-central

Fig. 1. Topographical map (Garmin MapSource®) highlighting important mines within Red Canyon, San Juan County, Utah, USA.

https://doi.org/10.1180/minmag.2017.081.094 Published online by Cambridge University Press

San Juan County, in southeastern Utah (Fig. 1). The Blue Lizard mine is situated on the northern ridge of Red Canyon, ~1 km to the northeast of the Markey mine and ~22 km southeast of Good Hope Bay on Lake Powell. Detailed historical and geological information on the Blue Lizard mine is described elsewhere (Kampf *et al.*, 2015), and is derived primarily from a report by Chenoweth (1993).

Redcanyonite is amongst the rarest of the uranyl sulfates found in the Blue Lizard mine and has so far been found only in a small (~0.5 m^2) area of the mine. Its rarity is probably due to a dependence on the availability of Mn^{2+} and co-existence with NH_4^+. Secondary uranium mineralization in Red Canyon is often localized and most prevalent within organic-rich beds that are laced with uraninite and sulfides. We infer the source of NH_4^+ is from decomposition of organic material, but were unable to identify the source of Mn^{2+}. The new mineral occurs intimately with ammoniozippeite in several specimens, which was previously only known as a synthetic phase. Other associated secondary minerals include bobcookite, brochantite, devilline, gypsum, johannite, posnjakite, natrozippeite, pentahydrite and pickeringite.

Physical and optical properties

Redcanyonite occurs as radial aggregates of needles and blades individually measuring up to 0.2 mm long; the aggregates are up to 1 mm in diameter (Figs 2 and 3). Crystals are flattened on {010} and elongated on [100], and exhibit the forms {001}, {010}, {101} and {10$\bar{1}$} (Fig. 4). Many crystals are twinned by 180° rotation on [100]. Crystals are translucent with a vitreous lustre, pale orange streak, and are non-fluorescent under both long-wave and shortwave ultraviolet illumination. The mineral is easily soluble in room-temperature dilute HCl. The Mohs hardness is ~2, estimated by the behaviour of crystals when broken. Crystals of redcanyonite are brittle with perfect {010} cleavage and uneven fracture. The density could not be measured due to the limited availability of material, and because it exceeds that of known heavy liquids. The calculated density is 4.633 g cm^{-3} based on the empirical formula, and 4.688 g cm^{-3} for the ideal formula.

Optically, redcanyonite is biaxial (+), with α = 1.725(3), β = 1.755(3) and γ = 1.850(5) (measured in white light). The measured 2V is 60(2)°, based on extinction data collected on a spindle stage and analysed using *EXCALIBRW* (Gunter *et al.*, 2004); the calculated 2V is 61.3°. Dispersion is very strong, $r < v$. The mineral is pleochroic with X = orange, Y = yellow and Z = orange; $Y << X < Z$. The optical orientation is $X = \mathbf{b}$, $Y \approx \mathbf{c}^*$, $Z \approx \mathbf{a}$.

The Gladstone-Dale compatibility, $1 - (K_p/K_c)$, is 0.001 (superior) for the ideal formula, and 0.065 (fair) for the empirical formula (Mandarino, 2007) using the value for $k(UO_3) = 0.134$, given by Larsen (1921).

Infrared spectroscopy

Attenuated total reflectance (ATR) Fourier-transform infrared (FTIR) spectra were obtained using a liquid N_2 cooled SENSIR Technologies IlluminatIR mounted to an Olympus BX51 microscope. An ATR objective was pressed into crystals of redcanyonite and measured from 4000 to 650 cm^{-1}. The infrared spectrum of redcanyonite is shown in Fig. 5,

FIG. 2. Spray of redcanyonite needles on brochantite and devilline. Horizontal field of view is ~0.6 mm.

https://doi.org/10.1180/minmag.2017.081.094 Published online by Cambridge University Press

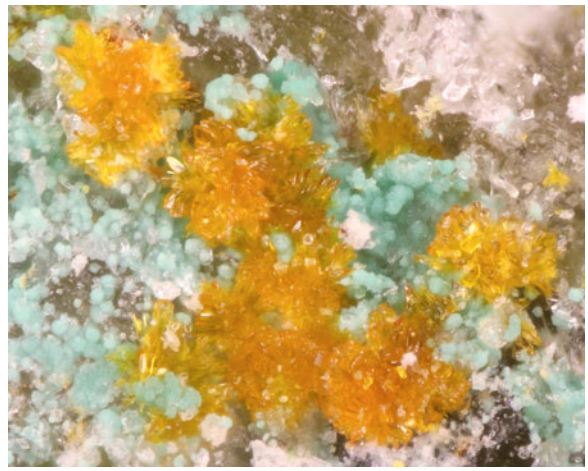

FIG. 3. Sprays of bladed redcanyonite with bluish-green devilline, and white pentahydrite. Horizontal field of view is ~1.2 mm.

and assignments are based on those of Čejka (1999). A series of broad bands observed between ~3500 cm^{-1} and ~2800 cm^{-1} are attributed to the ν O–H stretching vibrations of hydrogen-bonded water molecules, overlapped with N–H stretching vibrations from interlayer NH_4^+ molecules. Due to overlap, attributing specific assignments to these bands is difficult. Approximate O–H···O hydrogen donor–acceptor distances calculated from the observed stretching frequencies are in the range ~2.9 to 2.6 Å using the correlation function given by Libowitzky (1999) and correspond well to those measured by single-crystal X-ray diffraction. A weak band found at 1615 cm^{-1} is assigned as the ν_2 (δ)-bending vibration of hydrogen-bonded crystalline water. A medium strong band at 1408 cm^{-1} is assigned to the N–H bending vibration of NH_4^+ molecules (Pekov *et al.*, 2014).

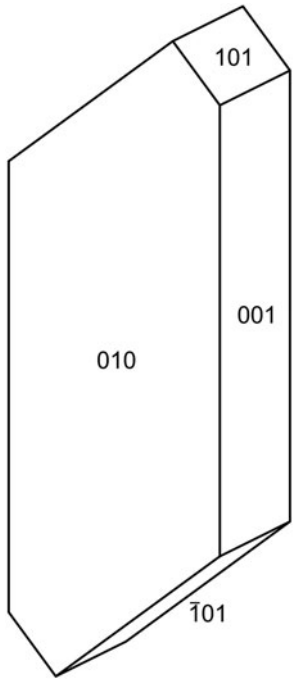

FIG. 4. Crystal drawing of redcanyonite; clinographic projection in non-standard orientation (*a* vertical).

Absorption bands at 1155, 1140 and 1084 cm^{-1} are assigned to the split triply degenerate ν_3 $(SO_4)^{2-}$ antisymmetric stretching vibration. The ν_1 $(SO_4)^{2-}$ symmetric stretch, which usually occurs between ~1100–1000 cm^{-1} is enveloped by the ν_3 $(UO_2)^{2+}$ antisymmetric stretch. The very strong antisymmetric ν_3 $(UO_2)^{2+}$ stretch occurs as a relatively broad band at 940 cm^{-1}. A weak band at 836 cm^{-1} is attributed to the ν_1 $(UO_2)^{2+}$ symmetric stretch, which although forbidden by selection rules, may be observed due to slight distortions. The uranyl U–O bond lengths inferred from the IR spectrum of redcanyonite using the empirical relation given by Bartlett and Cooney (1989) are 1.77 Å (ν_3) and 1.78 Å (ν_1).

Raman spectroscopy

The Raman spectrum of redcanyonite was taken using a Bruker Instruments Sentinel-785 laser head

https://doi.org/10.1180/minmag.2017.081.094 Published online by Cambridge University Press

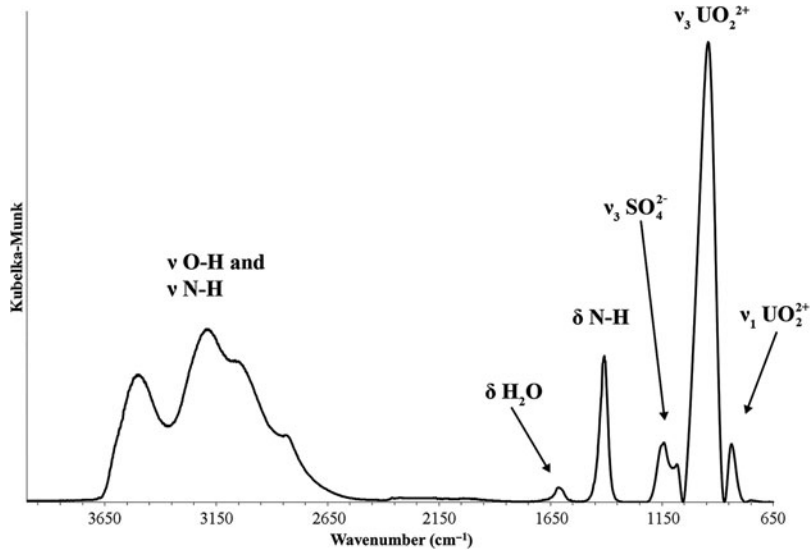

FIG. 5. Infrared spectrum (ATR) of redcanyonite in the region from 4000 to 600 cm^{-1}.

mounted on a Nikon Optiphot-2 microscope with Peltier-cooled integrated 785 nm diode laser, operated at 200 mW, 100 µm spot size and ~5 cm^{-1} resolution. The spectrometer was calibrated using software-controlled procedures (*Opus* software) from neon emission lines (wavelength calibration), and Tylenol® Raman bands (frequency calibration). A background correction was applied using the *Opus* software.

The Raman spectrum of redcanyonite is given in Fig. 6. The split triply degenerate ν_3 $(SO_4)^{2-}$ antisymmetric stretching vibrations occur as weak

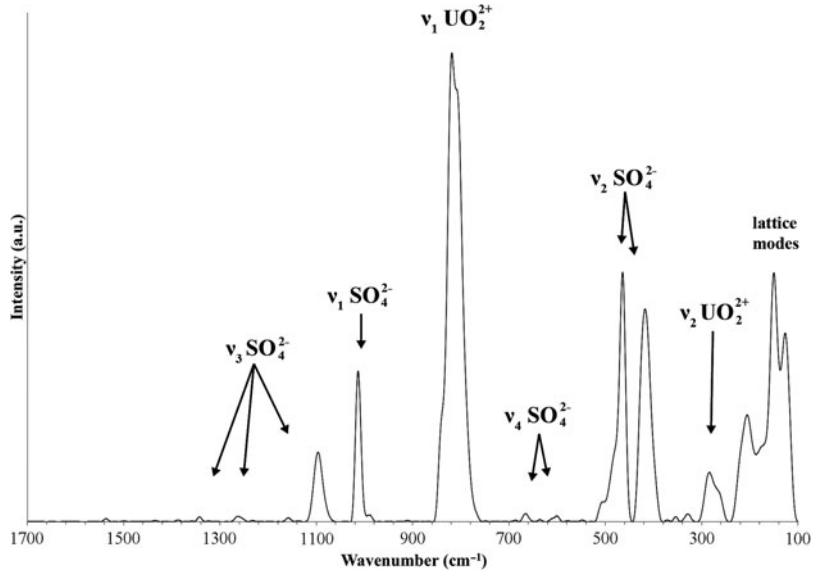

FIG. 6. Raman spectrum of redcanyonite, taken with a 785 nm laser.

https://doi.org/10.1180/minmag.2017.081.094 Published online by Cambridge University Press

bands at 1263, 1158 and 1097 cm^{-1}, and a medium intensity band at 1013 cm^{-1} is assigned to the $\nu_1 (SO_4)^{2-}$ symmetric stretching vibration. The $\nu_1 (UO_2)^{2+}$ symmetric stretching vibration is present as a very strong band at 819, with a shoulder at 809 cm^{-1}. Bartlett and Cooney (1989) provide an empirical relation to derive the approximate U–O_{yl} bond lengths from the band positions assigned to the $(UO_2)^{2+}$ stretching vibrations, which gives 1.79 Å (819 cm^{-1}) and 1.80 Å (809 cm^{-1}), in agreement with U–O_{yl} bond lengths from the X-ray data (see below).

Weak bands at 666 and 601 cm^{-1} are attributed to the split, triply degenerate $\nu_4(\delta)(SO_4)^{2-}$ bending vibrations, and those at 506, 464 and 418 cm^{-1} to the split doubly degenerate $\nu_2(\delta)(SO_4)^{2-}$ bending vibrations. Bands at 354 and 329 cm^{-1} are attributed to ν (U–$O_{equatorial}$) stretching vibrations, and bands found at 284 and 261 arise from $\nu_2(\delta)$U–O–U bending modes. The remaining bands at 206, 176, 150 and 127 cm^{-1} are assigned to external lattice vibration modes and UO_2^{2+} translations and rotations (Plášil *et al.*, 2010).

Chemical composition

Chemical analyses (five) were performed using a Cameca SX-50 electron microprobe (University of Utah), operating at an accelerating voltage of 15 kV, with a beam current of 10 nA and 5 μm spot diameter. Redcanyonite contains appreciable U, N, Mn and S, with some Zn and Cu. No other elements were detected. Matrix effects were accounted for using the *PAP* correction routine (Pouchou and Pichoir, 1985), and the analytical data are given in Table 1. The small and frail crystals were difficult to polish and exhibited moderate beam damage, resulting in low totals (96.22 wt.%). Due to the limited amount of material available the H_2O content was not measured and is instead calculated based on the structure. The presence of H_2O and NH_4 were confirmed by infrared spectroscopy. The empirical formula, calculated on the basis of 4 U and 24 O atoms per formula unit (apfu) is $(NH_4)_{2.02}(Mn_{0.49}Cu_{0.09}Zn_{0.06})_{\Sigma 0.64}H^+_{0.72}[(UO_2)_4O_4(S_{0.99}P_{0.01}O_4)_2](H_2O)_4$. The ideal formula is $(NH_4)_2Mn[(UO_2)_4O_4(SO_4)_2](H_2O)_4$ which requires $(NH_4)_2O$ 3.48, SO_3 10.68, MnO 4.73, UO_3 76.30, H_2O 4.81, for a total 100 wt.%.

Powder X-ray diffraction

Room-temperature powder diffraction data (Table 2) were recorded using a Rigaku R-Axis Rapid II curved imaging plate microdiffractometer with monochromated Mo*K*α radiation. A Gandolfi-like motion on the φ and ω axes was used to randomize diffraction from the sample. Observed *d*-values and intensities were derived by profile fitting using *JADE 2010* software (Materials Data, Inc.). Unit-cell parameters refined from the powder data using whole pattern fitting in *JADE 2010* are as follows: $a = 8.665(2)$, $b = 14.359(2)$, $c = 8.834(2)$ Å, $\beta = 104.190(5)°$ and $V = 1065.5(4)$ $Å^3$.

Single-crystal X-ray diffraction

Single crystal X-ray diffraction data were collected using an Apex II CCD-based detector and

TABLE 1. Data from electron microprobe analysis for redcanyonite, average of five analyses.

Constituent	Mean wt.%	Range	S.D.	Probe standard
$(NH_4)_2O$	3.41	2.84–4.20	0.51	Cr_2N (synth.)
P_2O_5	0.10	0.00–0.16	0.07	apatite
SO_3	10.28	9.45–10.77	0.63	celestine
MnO	2.26	1.72–2.87	0.46	rhodonite
CuO	0.46	0.11–0.71	0.25	Cu
ZnO	0.34	0.12–0.49	0.16	Zn
UO_3	74.27	73.13–75.13	0.80	UO_2 (synth.)
H_2O*	5.10	–	–	
Total	96.22			

*Calculated based on the structure
S.D. – standard deviation

https://doi.org/10.1180/minmag.2017.081.094 Published online by Cambridge University Press

TABLE 2. Powder X-ray data (d in Å) for redcanyonite.

I_{obs}	d_{obs}	d_{calc}	I_{calc}	hkl	I_{obs}	d_{obs}	d_{calc}	I_{calc}	hkl	I_{obs}	d_{obs}	d_{calc}	I_{calc}	hkl
21	8.55	8.5759	25	0 0 1	10	2.1151	2.1331	2	2 0 3	5	1.6542	1.6669	1	0 2 5
		7.2211	3	1 1 0			2.1315	1	$\bar{2}$ 0 4			1.6648	1	$\bar{1}$ 7 3
100	7.19	7.0775	100	0 2 0			2.0981	2	$\bar{4}$ 0 2			1.6541	1	$\bar{3}$ 7 1
		6.2018	5	$\bar{1}$ 1 1	20	2.0686	2.0697	8	$\bar{4}$ 2 1			1.6390	2	3 7 0
12	5.49	5.4587	7	0 2 1			2.0673	2	$\bar{3}$ 3 3			1.6304	1	$\bar{2}$ 8 1
7	4.271	4.2880	5	0 0 2			2.0566	2	2 6 0	4	1.6168	1.6146	1	1 5 4
15	4.161	4.1961	8	$\bar{2}$ 0 1			2.0519	2	0 2 4			1.6091	1	$\bar{5}$ 3 2
		4.1133	1	1 3 0			2.0424	2	2 2 3	8	1.5962	1.5948	3	$\bar{4}$ 6 1
		4.0820	1	$\bar{1}$ 1 2			2.0410	3	$\bar{2}$ 2 4			1.5867	1	0 6 4
6	3.942	3.8947	3	$\bar{1}$ 3 1	12	2.0159	2.0115	5	$\bar{4}$ 2 2			1.5816	1	$\bar{2}$ 6 4
7	3.661	3.6674	6	0 2 2			2.0018	1	$\bar{1}$ 3 4	9	1.5722	1.5744	3	$\bar{2}$ 8 2
33	3.600	3.6105	10	2 2 0			1.9903	1	3 5 0			1.5691	1	3 7 1
		3.5472	3	1 3 1	17	1.9670	1.9659	1	1 7 0			1.5678	1	$\bar{4}$ 6 2
		3.5388	21	0 4 0			1.9478	9	2 6 1			1.5649	3	2 4 4
56	3.453	3.4496	41	$\bar{2}$ 0 2			1.9405	3	$\bar{1}$ 7 1			1.5641	2	$\bar{2}$ 4 5
3	3.320	3.2712	5	0 4 1	6	1.9296	1.9328	1	4 0 1	13	1.5554	1.5515	3	4 4 2
72	3.112	3.1030	55	2 2 1			1.9315	1	$\bar{4}$ 0 3			1.5505	3	$\bar{4}$ 4 4
15	2.853	2.8586	12	0 0 3	3	1.8910	1.8928	2	1 7 1			1.5459	1	1 9 0
		2.8056	2	1 3 2			1.8645	1	4 2 1			1.5434	1	0 4 5
4	2.730	2.7293	1	0 4 2	9	1.8558	1.8633	1	$\bar{4}$ 2 3	5	1.5242	1.5334	2	$\bar{1}$ 9 1
		2.7052	2	$\bar{2}$ 4 1			1.8464	4	$\bar{4}$ 4 1			1.5186	1	$\bar{3}$ 7 3
		2.6896	1	2 0 2	10	1.8324	1.8269	2	2 4 3			1.5148	1	3 5 3
		2.6874	2	$\bar{2}$ 0 3			1.8259	1	$\bar{2}$ 4 4	3	1.4985	1.5045	1	0 8 3
		2.6826	1	1 5 0			1.8196	4	0 6 3			1.4921	1	$\bar{1}$ 7 4
23	2.657	2.6506	17	0 2 3	8	1.7941	1.8047	1	$\bar{4}$ 4 2			1.4756	1	$\bar{1}$ 9 2
		2.6191	4	$\bar{1}$ 5 1			1.7850	2	$\bar{3}$ 5 3			1.4379	1	$\bar{6}$ 0 1
		2.5142	1	2 2 2			1.7736	1	2 6 2			1.4339	1	1 9 2
		2.5052	1	1 5 1	9	1.7540	1.7694	2	0 8 0			1.4293	1	0 0 6
21	2.491	2.4702	14	$\bar{2}$ 4 2			1.7496	3	1 7 2	17	1.4034	1.4089	1	$\bar{6}$ 2 2
4	2.400	2.4070	1	3 3 0			1.7448	3	2 0 4			1.4028	2	2 6 4
		2.3592	3	0 6 0			1.7436	2	$\bar{2}$ 0 5			1.4022	2	$\bar{2}$ 6 5
		2.2747	2	0 6 1			1.7423	1	$\bar{1}$ 5 4			1.4010	1	0 2 6
		2.2700	1	$\bar{3}$ 1 3	13	1.7291	1.7329	1	0 8 1			1.3993	1	6 0 0
		2.2261	1	1 3 3			1.7263	3	4 0 2			1.3987	1	$\bar{6}$ 0 3
13	2.232	2.2237	7	0 4 3			1.7248	3	$\bar{4}$ 0 4			1.3965	1	1 5 5
		2.2005	1	3 3 1			1.7152	1	0 0 5			1.3931	1	4 6 2
		2.1985	1	1 5 2								1.3924	1	$\bar{4}$ 6 4

(continued)

TABLE 2. (*contd.*)

I_{obs}	d_{obs}	d_{calc}	I_{calc}	*hkl*	I_{obs}	d_{obs}	d_{calc}	I_{calc}	*hkl*	I_{obs}	d_{obs}	d_{calc}	I_{calc}	*hkl*
11	2.1621	2.1643	6	$\bar{4}$ 0 1	17	1.6977	1.6964	2	3 5 2					
		2.1440	1	0 0 4			1.6954	1	$\bar{4}$ 4 3	7	1.3772	1.3727	1	6 2 0
		2.1402	1	$\bar{2}$ 4 3			1.6940	4	2 2 4			1.3722	2	$\bar{6}$ 2 3
							1.6930	5	$\bar{2}$ 2 5			1.3711	1	3 9 0
					15	1.6780	1.6771	4	4 2 2			1.3699	1	$\bar{4}$ 8 1
							1.6758	4	$\bar{4}$ 2 4					

Mo*K*α X-rays from a microfocus source mounted to a Bruker Quazar three-circle diffractometer. Corrections for Lorentz, polarization and background effects were made using the Bruker program *SAINT*. A multi-scan semi-empirical absorption correction was applied using equivalent reflections in *SADABS-2012*. An initial structure model was obtained by the charge-flipping method using *SHELXT* (Sheldrick, 2015) in space group *C*2/*m*. The *JANA2006* software package (Petříček *et al.*, 2014) was used to refine the structure of redcanyonite on the basis of F^2 for unique reflections, to a final R_1 of 3.75% for 1079 reflections with $I_{obs} > 3\sigma I$. Details regarding the data collection and refinement results are given in Table 3, and atomic coordinates and displacement parameters in Table 4. The crystallographic information files have been deposited with the Principal Editor of *Mineralogical Magazine* and are available as Supplementary material (see below). Hydrogen atoms could not be located due to weak X-ray scattering, however hydrogen-bonding information is proposed on the basis of selected interatomic distances given in Table 5, and a bond-valence analysis in Table 6. Uranium, S, Mn and O atoms of the sheet were refined using harmonic atomic displacement parameters, and the remaining atoms (interlayer N and Ow) were refined isotropically. Due to the small size of the crystals, weak and diffuse reflections requiring doubling of the *c* parameter are present in the diffraction pattern, but attempts to integrate and refine these reflections were difficult, and refinement in a cell with $c = \sim 17$ Å led to overall unsatisfactory results. The crystal of redcanyonite chosen for diffraction was twinned, and applying the twin law ($\bar{1}$,0,½/0,$\bar{1}$,0/0,0,1) led to an improvement in the *R* factor by ~5%.

Features of the crystal structure

The structure of redcanyonite contains one symmetrically distinct U site, with one S site, one Mn site and seven O sites. Two multiply-bonded oxygen atoms are arranged in a linear fashion about each uranium atom, forming the uranyl unit $(UO_2)^{2+}$. Five O anions sit at the equatorial vertices of a uranyl pentagonal bipyramid, capped on top and bottom by uranyl oxygen atoms O_{yl}. Each sulfur cation (S^{6+}) is tetrahedrally coordinated, with < S–O > bond lengths ranging from 1.44 to 1.49 Å.

https://doi.org/10.1180/minmag.2017.081.094 Published online by Cambridge University Press

TABLE 3. Data collection and structure-refinement details for redcanyonite.

Diffractometer	Bruker Quazar II with Apex II detector
X-ray radiation/power	Mo$K\alpha$ ($\lambda = 0.71075$ Å)/50 kV, 60 mA
Temperature (K)	298(2)
Structural formula	$(NH_4)_2Mn_{0.874}[(UO_2)_4O_4(SO_4)_2](H_2O)_4$
Space group	$C2/m$
Unit-cell dimensions (Å)	$a = 8.6572(17)$ $b = 14.155(3)$ $c = 8.8430(19)$ $\beta = 104.117(18)$
V (Å^3)	1050.9(4)
Z	2
$D_{calc.}$ (g cm^{-3})	4.665 (for the above formula)
Absorption coefficient (mm^{-1})	31.54
$F(000)$	1256
Crystal size (mm)	0.030 × 0.025 × 0.002
θ range	2.37 to 28.52°
Index ranges	$-11 \le h \le 11$, $-19 \le k \le 19$, $-11 \le l \le 11$
Reflections collected/unique	6353/1382; $R_{int} = 0.0545$
Reflections with $I_{obs} > 3\sigma(I)$	1079
Completeness to θ = 28.52°	98%
Refinement method	Full-matrix least-squares on F^2
Parameters (restraints/constraints)	73 (0/0)
GoF (obs/all)	1.21/1.30
R (obs), wR (obs)	0.0375, 0.0953
R (all), wR (all)	0.0493, 0.1013
Largest diff. peak/hole (e^- Å^{-3})	+1.69 /–1.32
Twin matrix	$\bar{1}$ 0 ½, 0 $\bar{1}$ 0, 0 0 1
Twin fractions	0.452/0.548

The uranyl pentagonal bipydramids and sulfate tetrahedra are linked to form the well-known zippeite type (Burns, 2005). It consists of zigzag chains of uranyl pentagonal bipyramids two-polyhedra wide that extend along [100], where individual chains link to form a sheet by sharing equatorial vertices with sulfate tetrahedra. Each sulfate tetrahedron links four unique bipyramids (two bipyramids of two separate chains) and propagates the zippeite-type sheet along [001]. Individual sheets stack parallel to (010), which corresponds to the excellent cleavage. Sheets are linked through a network of H bonds that emanate from interstitial water and ammonium groups (Fig. 7). Each ammonium group bonds to two water molecules within the interlayer (Ow1), four O_{yl} atoms (two from each sheet, O4 and O5), and two equatorial oxygen atoms (one from each sheet, O2) which are part of the SO_4 tetrahedra. Additional linkages between sheets are made through $Mn(H_2O)_2O_4$ octahedra, where the apex of each octahedron correspond to two water molecules of the interlayer (Ow2), and four O atoms of uranyl ions (O4).

According to the chemical analyses, redcanyonite contains variable Mn^{2+}, Cu^{2+} and Zn^{2+} in the interlayer and site-scattering refinement performed during the final cycles of refinement gives 0.874 Mn apfu. Chemical and configurational variability is a recurring feature in natural zippeite-group phases (e.g. Brugger *et al.*, 2003; Plášil *et al.*, 2011*a*,*b*, 2013, 2014; Plášil and Škoda, 2015) and synthetic phases (Burns *et al.*, 2003; Peeters *et al.*, 2008). Similarly, Frondel *et al.* (1976) observed considerable solid solution between end-member compositions of synthetic NH_4, Ni, Co and Mg-containing zippeites. It is also common within this group for phases with similar compositions to have slightly different interlayer arrangements (Plášil *et al.*, 2013). The structure of redcanyonite is most closely related to

https://doi.org/10.1180/minmag.2017.081.094 Published online by Cambridge University Press

TABLE 4. Atomic coordinates and displacement parameters (U_{eq}, U_{iso}, in Å^2) for redcanyonite.

Atoms	*x*	*y*	*z*	U_{eq}/U_{iso}	U^{11}	U^{22}	U^{33}	U^{12}	U^{13}	U^{23}
U1	0.83148(14)	0.23257(3)	0.33016(4)	0.02408(17)	0.0205(3)	0.0358(3)	0.0152(2)	−0.0001(4)	0.0029(3)	−0.00016(15)
Mn1*	0	0.2501(3)	0	0.0233(10)	0.024(3)	0.032(3)	0.021(2)	0	0.0083(18)	0
S1	0	0	½	0.0254(16)	0.0190(14)	0.038(2)	0.0164(14)	0	0.011	0
O1	−0.0725(11)	0.1860(8)	0.0980(11)	0.032(3)	0.026(5)	0.047(7)	0.022(5)	−0.002(4)	0.006(4)	−0.002(4)
O2	−0.1192(11)	0.3080(8)	−0.0998(11)	0.035(3)	0.019(5)	0.057(7)	0.022(5)	0.004(5)	−0.008(4)	−0.007(5)
O3	1.109(4)	0.2528(6)	0.4112(9)	0.028(3)	0.014(5)	0.050(5)	0.017(3)	−0.004(4)	0.002(9)	0.000(3)
O4	0.8438(13)	0.1070(6)	0.3655(9)	0.029(3)	0.027(5)	0.034(5)	0.023(4)	−0.010(5)	0.000(5)	−0.001(3)
O5	0.8148(14)	0.3549(6)	0.2738(10)	0.034(3)	0.030(5)	0.042(5)	0.029(4)	0.005(5)	0.008(5)	0.000(4)
N1	0.541(4)	0	0.217(3)	0.082(7)						
Ow1	0.230(3)	0	−0.022(3)	0.096(7)						
Ow2	0.1163(19)	0	0.3279(17)	0.045(4)						

*Refined occupancy of Mn1 is 0.218

plavnoite (Plášil *et al.*, 2017), ammoniozippeite (Kampf *et al.*, 2018), and other monoclinic members of the zippeite group containing M^{2+}. It is the first naturally occurring zippeite-group mineral that contains NH_4^+ groups in the interlayer, and differs from others by the unique arrangement of Mn^{2+} and NH_4^+ (Fig. 8).

Refinement indicates that structural units in redcanyonite have the composition $[(UO)_4O_4(SO_4)_2]^{4-}$, although some sheets in zippeite minerals contain hydroxyl. The calculated bond-valence sum of the μ_3-bridging oxygen atom O3 is 1.87 valence units (vu), inconsistent with OH^-. Where this site contains OH^- in other zippeite-group phases, sums range between 1.27–1.4 vu (e.g. Burns *et al.*, 2003; Brugger *et al.*, 2003; Plášil *et al.*, 2011*a*,*b*; Plášil and Škoda, 2015). The lack of evidence for sheet hydroxyl in redcanyonite in addition to partially occupied interlayer constituents may suggest that minor H^+ (as H_3O+) is associated with interlayer water molecules to provide the charge balance. Such is the case for natural zippeite (Plášil *et al.*, 2011*b*), with an interlayer composition of $K_{1.85}H^+_{0.15}$. Similarly, the interlayer composition of the related zippeite-group phase sejkoraite-(Y) (Plášil *et al.*, 2011*a*) is $(Y_{1.98}Dy_{0.24})_{\Sigma 1.82}H^+_{0.34}$, where excess H^+ accounts for charge-balance deficiencies from partially occupied M^{3+}. Some complications with this assignment arise due to artefacts from site-scattering refinement and inadequacies of microprobe analyses, although, that zippeite-group members are formed under acidic conditions supports the existence of H_3O^+. We cannot rule out partial sheet-protonation in redcanyonite, however, as in other zippeite-group minerals the charge balancing mechanism for partial Mn occupancy in redcanyonite may involve excess H^+ (as H_3O^+) dispersed in the interlayer, or excess NH_4^+.

Yellow crystals of ammoniozippeite are found to occur intimately with redcanyonite in some of the samples under study, and structure refinement suggests ammoniozippeite crystallizes in a cell related to redcanyonite, but with vacancy at the corresponding Mn site. Its structural sheet is not protonated; consistent with the observations by Burns *et al.* (2003) for synthetic NH_4-zippeite designated 'SZIPPNH$_4$I'. Thus, interlayer compositions between redcanyonite and ammoniozippeite may form a solid-solution series, which can be written as $(NH_4)_{2+2x}Mn_{1-x}$, assuming that no sheet protonation or interlayer H_3O^+ is present. The formula of redcanyonite from the structure refinement is $(NH_4)_2Mn_{0.874}[(UO_2)_4O_4(SO_4)_2](H_2O)_4$

https://doi.org/10.1180/minmag.2017.081.094 Published online by Cambridge University Press

TABLE 5. Selected interatomic distances (Å) in the structure of redcanyonite.

U1–O1	2.485(16)	N1–Ow1	2.93(5)
U1–O2	2.456(28)	N1–Ow1	2.99(5)
U1–O3	2.351(35)	N1–O2 (×2)	3.043(2)
U1–O3	2.237(12)	N1–O4 (×2)	3.035(3)
U1–O3	2.223(35)	N1–O5 (×2)	2.964(3)
U1–O4	1.803(8)	<NH_4–O>	3.00
U1–O5	1.798(8)		
<U–O_{yl}>	1.801		
<U–O_{eq}>	2.350	Hydrogen bonds	
		Ow1···O1 (×2)	2.966(16)
Mn1–O4 (×4)	2.180(16)	Ow1···O2 (×2)	3.163(19)
Mn1–Ow2 (×2)	2.019(22)	Ow2···O5 (×2)	2.793(17)
<Mn–O>	2.126	Ow2···O4 (×2)	3.051(16)
		Ow2···O4 (×2)	2.890(19)
S1–O1 (×2)	1.495(13)	<Ow···O>	2.973
S1–O2 (×2)	1.439(15)		
<S–O>	1.470		

with $Z = 2$ and $D_{calc} = 4.665$ g cm^{-3}, which has a net –0.25 charge. With this in mind, the structural formula can be balanced with respect to solid solution towards ammoniozippeite as $(NH_4)_{2.26}Mn_{0.874}[(UO_2)_4O_4(SO_4)_2](H_2O)_4$. However, charge balance may also be met by calling upon excess interlayer H^+ $(NH_4)_2Mn_{0.874}H^+_{0.26}[(UO_2)_4O_4(SO_4)_2](H_2O)_4$. Either assignment is plausible in the absence of H-atom positions, and we can neither confirm nor deny the presence of H_3O^+ or excess NH_4^+ in the interlayer from the X-ray data. Future work requires application of neutron diffraction or spectroscopic techniques sensitive to H atoms to resolve the role of H_3O^+ in redcanyonite and other zippeite-group minerals.

Conclusions

Humans can have a significant influence on Earth's mineral diversity (Hazen *et al.*, 2017). We owe ourselves partial credit for the occurrence of chemically and structurally complex uranyl sulfate minerals found in Red Canyon. Human activity (mining and removal of rock) has accelerated secondary mineralization of uranium there, and has allowed us to study the formation of uranyl sulfate structures. Redcanyonite has formed because mining facilitated interactions between Mn^{2+}, possibly derived from primary oxide or sulfide sources, and NH_4^+ formed by decomposition of organic material. Such "human mediated mineralogy" (Hazen *et al.*, 2017) has produced

TABLE 6. Bond-valence analysis (valence units, vu) for redcanyonite.

	U1	Mn1	S1	N1 (NH_4^+)	Σ_{anion}	O assignment	Expected H bonds
O1	0.40		1.41 × 2↓		1.81	O	(0.2 × 1)
O2	0.42		1.63 × 2↓	0.11 × 2↓	2.16	O	
O3	0.69, 0.67, 0.52				1.88	O	
O4	1.67	0.35 × 4↓		0.11 × 2↓	2.13	yl O	
O5	1.69			0.13 × 2↓	1.82	yl O	(0.2 × 1)
Ow1				0.12, 0.15	0.27	H_2O	(0.8 × 2)
Ow2		0.51 × 2↓			0.51	H_2O	(0.8 × 2)
Σ_{cation}	6.06	2.42	6.08	0.97			

Bond-valence parameters for U^{6+}–O, Mn^{2+}–O, S^{6+}–O from Gagné and Hawthorne (2015); and NH_4^+···O from García-Rodríguez *et al.* (2000). Expected hydrogen bond-valence contributions are included, with values for donor (D—H, ~0.8 vu) and acceptor (H—A, ~0.2 vu) bond strengths taken from Hawthorne and Schindler (2008).

https://doi.org/10.1180/minmag.2017.081.094 Published online by Cambridge University Press

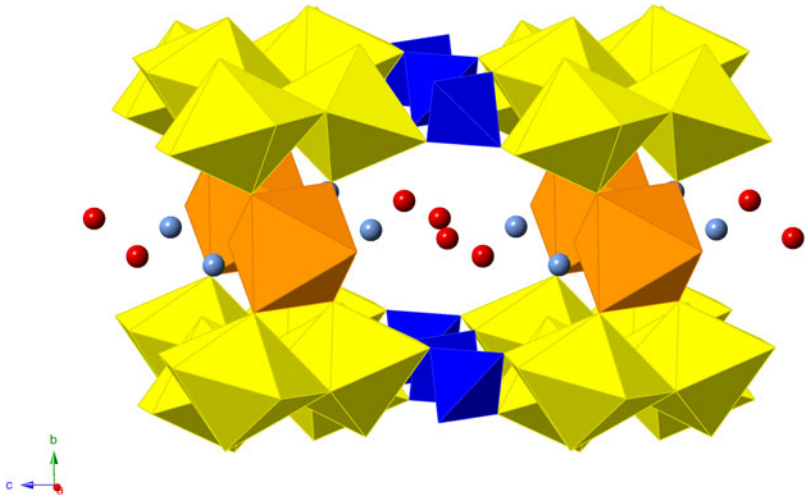

FIG. 7. Polyhedral representation of the structure of redcanyonite. Uranium (yellow), sulfur (blue), manganese (orange), nitrogen (light blue), oxygen (red).

unique geochemical conditions in Red Canyon, and recognizing them is useful from an environmental standpoint. For example, successful remediation of sulfide-rich uranium mine tailings, or storage of actinide-bearing wastes in a geological repository are both dependent on preventing interactions between actinides, anthropogenical materials and acidic sulfate groundwater. The Red Canyon region has, and will probably continue, to provide significant advances to our understanding of uranyl minerals and uranyl sulfates formed by alteration of underground mine workings.

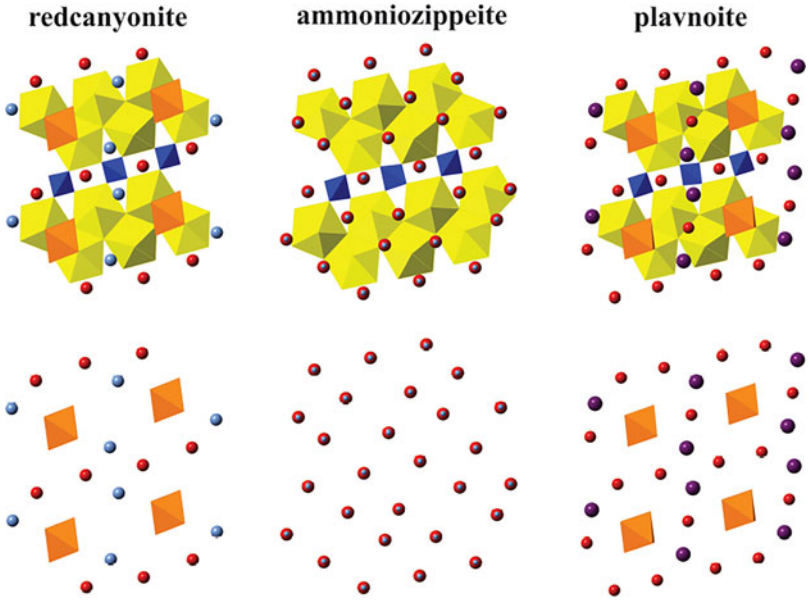

FIG. 8. A comparison of interlayer arrangement in redcanyonite, ammoniozippeite and plavnoite as viewed down *b*. Manganese (orange), nitrogen (light blue), potassium (purple), oxygen (red), uranium (yellow) and sulfur (blue).

https://doi.org/10.1180/minmag.2017.081.094 Published online by Cambridge University Press

TABLE 7. A comparison of related phases with the zippeite sheet topology.

	Redcanyonite	Ammoniozippeite	'SZIPPNH4I'	Zippeite	Plavnoite	Mn-K-zippeite
Locality	Red Canyon, USA	Burro mine, USA	synthetic	Jáchymov, CZ	Jáchymov, CZ	synthetic
Reference	This work	Kampf *et al.* (2018)	Burns *et al.* (2003)	Plášil *et al.* (2011*b*)	Plášil *et al.* (2017)	Peeters *et al.* (2008)
Structural unit	$[(UO_2)_4O_4(SO_4)_2]$	$[(UO_2)_2O_2(SO_4)]$	$[(UO_2)_4O_4(SO_4)_2]$	$[(UO_2)_2O_2(SO_4)(OH)_2]$	$[(UO_2)_2O_2(SO_4)]$	$[(UO_2)_2O_2(SO_4)]$
M (ideal)	$(NH_4)_2Mn$	$(NH_4)_2$	$(NH_4)_4$	K_2	$K_{0.8}Mn_{0.6}$	$Mn_{0.75}K_{0.5}$
M (refined)	$(NH_4)_2Mn_{0.874}$	$(NH_4)_2$	$(NH_4)_4$	$K_{1.85}$	$K_{0.53}Mn_{0.57}$	$Mn_{0.75}K_{0.5}$
M (meas.)	$(NH_4)_{2.02}(Mn_{0.49}Cu_{0.09}Zn_{0.06})_{\Sigma 0.64}$	$(NH_4)_{1.97–1.99}$	–	$(K_{1.73}Fe_{0.04}Ca_{0.02})_{\Sigma 1.82}$	$K_{0.75}(Mn_{0.5}Zn_{0.04}Ni_{0.03}Mg_{0.02})_{\Sigma 0.59}$	$Mn_{0.68}K_{0.19}$
Space group	*C*2/*m*	*Ccmb*	*C*2/*m*	*C*2/*m*	*C*2/*c*	*C*2/*c*
a (Å)	8.6572(17)	8.7944(3)	8.6987(15)	8.7802(6)	8.6254(16)	8.661(6)
b (Å)	14.155(3)	14.3296(7)	14.166(2)	13.9903(12)	14.258(3)	14.375(8)
c (Å)	8.8430(19)	17.1718(12)	17.847(4)	8.8630(6)	17.703(1)	17.705(12)
β (°)	104.117(18)	–	104.117(4)	104.524(7)	104.052(18)	104.12(5)
V (Å^3)	1050.9(4)	2164.0(2)	2132.9(3)	1053.92(12)	2122.0(8)	2138(2)
Z	2	8	2	2	8	8
Strongest lines	8.576/25	8.64/7	8.656/15	8.578/21	8.595/27	8.858/20
in PXRD, calc.	7.078/100	7.17/100	7.083/100	6.998/100	7.133/100	5.551/43
from structure	3.567/34	3.580/21	3.541/15	3.500/26	3.565/25	3.594/100
(*d*/rel. int.)	3.453/41	3.489/42	3.474/36	3.476/19	3.446/36	3.112/81
	3.103/55	3.138/63	3.119/49	3.113/42	3.104/47	2.862/26

Acknowledgements

We thank two anonymous reviewers for valuable comments that improved the quality of this manuscript. Support for this work is provided by the Chemical Sciences, Geosciences and Biosciences Division, Office of Basic Energy Sciences, Office of Science, U.S. Department of Energy, Grant No. DE-FG02-07ER15880. We thank the ND Energy Materials Characterization Facility for use of the single-crystal X-ray diffraction and Raman spectroscopy instruments. A portion of this study was funded by the John Jago Trelawney Endowment to the Mineral Sciences Department of the Natural History Museum of Los Angeles County. Jakub Plášil thanks support from GACR, grant no. 17-09161S.

Supplementary material

To view supplementary material for this article, please visit https://doi.org/10.1180/minmag.2017.081.094

References

Bartlett, J.R. and Cooney, R.P. (1989) On the determination of uranium-oxygen bond lengths in dioxouranium(VI) compounds by Raman spectroscopy. *Journal of Molecular Structure*, **193**, 295–300.

Brugger, J., Meisser, N. and Burns, P.C. (2003) Contribution to the mineralogy of acid drainage of uranium minerals: marécottite and the zippeite-group. *American Mineralogist*, **88**, 676–685.

Brugger, J., Wallwork, K.S., Meisser, N., Pring, A., Ondruš, P. and Čejka, J. (2006) Pseudojohannite from Jáchymov, Musonoï and La Creusaz: A new member of the zippeite-group. *American Mineralogist*, **91**, 929–936.

Burns, P.C. (2005) U^{6+} minerals and inorganic compounds: insights into an expanded structural hierarchy of crystal structures. *Canadian Mineralogist*, **43**, 1839–1894.

Burns, P.C., Deely, K.M. and Hayden, L.A. (2003) The crystal chemistry of the zippeite group. *Canadian Mineralogist*, **41**, 687–706.

Čejka, J. (1999) Infrared spectroscopy and thermal analysis of the uranyl minerals. Pp. 521–622 in: *Uranium: Mineralogy, Geochemistry and the Environment* (P.C. Burns and R.C. Ewing, editors). Reviews in Mineralogy & Geochemistry, **38**. Mineralogical Society of America, Washington DC.

Chenoweth, W.L. (1993) *The geology and production history of the uranium deposits in the White Canyon mining district, San Juan County, Utah*. Miscellaneous Publication 93-3, Utah Geological Survey, Salt Lake City, Utah, USA.

Finch, R.J. and Murakami, T. (1999) Systematics and paragenesis of uranium minerals. Pp. 91–179 in: *Uranium: Mineralogy, Geochemistry and the Environment* (P.C. Burns and R.C. Ewing, editors). Reviews in Mineralogy & Geochemistry, **38**. Mineralogical Society of America, Washington DC.

Frondel, C., Ito, J., Honea, R.M. and Weeks, A.M. (1976) Mineralogy of the zippeite group. *Canadian Mineralogist*, **14**, 429–436.

Gagné, O.C. and Hawthorne, F.C. (2015) Comprehensive derivation of bond-valence parameters for ion pairs involving oxygen. *Acta Crystallographica*, **B71**, 562–578.

García-Rodríguez, L., Rute-Pérez, Á., Piñero, J.R., González-Silgo, C. (2000) Bond-valence parameters for ammonium-anion interactions. *Acta Crystallographica*, **B56**, 565–569.

Garrels, R.M. and Christ, C.L. (1959) Behavior of uranium minerals during oxidation. Pp 81–89 in: *Geochemistry and Mineralogy of the Colorado Plateau* (R.M. Garrels and E.S. Larsen, editors). Uranium Ores. U.S. Geol. Survey Professional Paper, **320**.

Gunter, M.E., Weaver, R., Bandli, B.R., Bloss, F.D., Evans, S.H. and Su, S.C. (2004) Results from a McCrone spindle stage short course, a new version of ECXCALIBR, and how to build a spindle stage. *The Microscope*, **52**, 23–39.

Hawthorne, F.C. and Schindler, M. (2008) Understanding the weakly bonded constituents in oxysalt minerals. *Zeitschrift für Kristallographie*, **223**, 41–68.

Hazen, R.M., Grew, E.S., Origlieri, M.J. and Downs, R.T. (2017) On the mineralogy of the "Anthropocene Epoch". *American Mineralogist*, **102**, 595–611.

Kampf, A.R., Plášil, J., Kasatkin, A.V. and Marty, J. (2015) Bobcookite, $NaAl(UO_2)_2(SO_4)_4 \cdot 18H_2O$ and wetherillite, $Na_2Mg(UO_2)_2(SO_4)_4 \cdot 18H_2O$, two new uranyl sulfate minerals from the Blue Lizard mine, San Juan County, Utah, USA. *Mineralogical Magazine*, **79**, 695–714.

Kampf, A.R., Plášil, J., Olds, T.A., Nash, B.P. and Marty, J. (2018) Ammoniozippeite, a new uranyl sulfate mineral from the Blue Lizard mine, San Juan County, Utah, and the Burro mine, San Miguel County, Colorado, USA. *The Canadian Mineralogist*, **56**, 235–245.

Langmuir, D. (1978) Uranium solution-mineral equilibria at low temperatures with applications to sedimentary ore deposits. *Geochimica et Cosmochimica Acta*, **42**, 547–569.

Larsen, E.S. (1921) *The Microscopic Determination of the Nonopaque Minerals*. U.S. Geological Survey, Bulletin 679.

Libowitzky, E. (1999) Correlation of O–H stretching frequencies and O–H···O hydrogen bond lengths in minerals. *Monatshefte für Chemie*, **130**, 1047–1059.

Mandarino, J.A. (2007) The Gladstone-Dale compatibility of minerals and its use in selecting mineral species for further study. *Canadian Mineralogist*, **45**, 1307–1324.

Peeters, M.O., Vochten, R. and Blaton, N. (2008) The crystal structures of synthetic potassium-transition metal zippeite-group phases. *Canadian Mineralogist*, **46**, 173–182.

Pekov, I.V., Krivovichev, S.V., Yapaskurt, V.O., Chukanov, N.V. and Belakovskiy, D.I. (2014) Beshtauite, $(NH_4)_2(UO_2)(SO_4)_2{\cdot}2H_2O$, a new mineral from Mount Beshtau, Northern Caucasus, Russia. *American Mineralogist*, **99**, 1783–1787.

Petříček, V., Dušek, M. and Palatinus, L. (2014) Crystallographic computing system Jana 2006: general features. *Zeitschrift für Kristallographie*, **229**, 345–352.

Plášil, J. (2014) Oxidation-hydration weathering of uraninite: The current state-of-knowledge. *Journal of Geosciences*, **59**, 99–114.

Plášil, J. (2015) Crystal structure refinement of pseudojohannite, $Cu_3(OH)_2$ $[(UO_2)_4O_4(SO_4)_2](H_2O)_{12}$, from the type locality – Jáchymov, Czech Republic. *Journal of Geosciences*, **60**, 123–127.

Plášil, J. and Škoda, R. (2015) New crystal-chemical data for marécottite. *Mineralogical Magazine*, **79**, 649–660.

Plášil, J., Buixaderas, E., Čejka, J., Sejkora, J., Jelička, J. and Novák, M. (2010) Raman spectroscopic study of the uranyl sulphate mineral zippeite: low wavenumber and U–O stretching regions. *Analytical and Bioanalytical Chemistry*, **397**, 2703–2715.

Plášil, J., Dušek, M., Novák, M., Čejka, J., Císařová, I. and Škoda, R. (2011*a*) Sejkoraite-(Y), a new member of the zippeite group containing trivalent cations from Jáchymov (St. Joachimsthal), Czech Republic: description and crystal structure refinement. *American Mineralogist*, **96**, 983–991.

Plášil, J., Mills, S.J., Fejfarová, K., Dušek, M., Novák, M., Škoda, R., Čejka, J. and Sejkora, J. (2011*b*) The crystal structure of natural zippeite, $K_{1.85}H^{+}_{0.15}[(UO_2)_4O_2(SO_4)_2(OH)_2](H_2O)_4$, from Jáchymov, Czech Republic. *Canadian Mineralogist*, **49**, 1089–1103.

Plášil, J., Fejfarová, K., Škoda, R., Dušek, M., Čejka, J. and Marty, J. (2013) The crystal structure of magnesiozippeite, $Mg[(UO_2)_2O_2(SO_4)](H_2O)_{3.5}$, from East Saddle Mine, San Juan County, Utah (U.S. A.). *Mineralogy and Petrology*, **107**, 211–219.

Plášil, J., Dušek, M., Čejka, J. and Sejkora, J. (2014) The crystal structure of rabejacite, the Ca^{2+}-dominant member of the zippeite group. *Mineralogical Magazine*, **57**, 1249–1263.

Plášil, J., Škácha, P., Sejkora, J., Kampf, A.R., Škoda, R., Čejka, J., Hloušek, J., Kasatkin, A.V., Pavlíček, R. and Babka, K. (2017) Plavnoite, a new K–Mn member of the zippeite group from Jáchymov, Czech Republic. *European Journal of Mineralogy*, **29**, 117–128.

Plášil, J., Petříček, V., Mills, S.J., Favreau, G. and Galea-Clolus, V. (2018) Zippeite from Cap Garonne, France: an example of reticular twinning. *Zeitschrift für Kristallographie-Crystalline Materials*, **233**(12), 861–865.

Pouchou, J.L. and Pichoir, F. (1985) "PAP" (φρZ) procedure for improved quantitative microanalysis. Pp. 104–106 in: *Microbeam Analysis* (J.T. Armstrong, editor). San Francisco Press, San Francisco, California.

Sheldrick, G.M. (2015) SHELXT – Integrated space-group and crystal-structure determination. *Acta Crystallographica*, **A71**, 3–8.

https://doi.org/10.1180/minmag.2017.081.094 Published online by Cambridge University Press